Engineering Structures 254 (2022) 113781

Contents lists available at ScienceDirect

Engineering Structures

journal homepage: www.elsevier.com/locate/engstruct

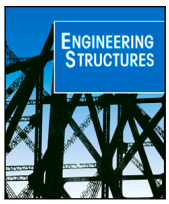

Control of the bridge span vibration with high coefficient passive damper. Theoretical consideration and application

Krzysztof Zoltowski *, Anna Banas, Mikolaj Binczyk, Przemyslaw Kalitowski

Gdank University of Technology, Narutowicza 11/12, 80-233, Gdansk, Poland

ARTICLE INFO

Keywords:
Footbridge dynamic
Human-induced vibration
Damping
Dynamic analysis
Dynamic response

ABSTRACT

The research was carried out due to the problem of vibration on the lively pedestrian drawbridge across the Motlawa River in the city of Gdansk. In the design stage, the main span of the footbridge showed unfavorable dynamic properties, which may create a comfort problem for pedestrians. The first vertical bending eigenfrequency was recognized as 1.64 Hz. The original design of the footbridge was equipped with a driving cylinder to operate opening of the drawbridge. It was installed between the abutment and the pylon (integrated part of the span). Based on numerical calculations, it turned out that its high overdamping ratio can raise the value of the first vertical natural frequency to the level where pedestrian action has a low influence on the dynamic excitation of the span. It should be noted, the solution does not affect the behavior of the structure under static loads. Therefore, it was decided to modify the existing hydraulic driving cylinder to become a damper also. Analytical and numerical modeling was performed to establish an appropriate range of damper constant values. Finally, this idea was implemented in the structure. The theoretically defined effects of introducing a high ratio damper have been practically confirmed during the field test. The first vertical natural frequency of the span was shifted from 1.64 Hz to 3.1 Hz. The paper presents the work related to the solution of a specific case. However, the presented idea can be used in a wide spectrum of structures subjected to dynamic excitation. In practice, an external damper enables the change of a "static scheme" of the structure in the selected range of dynamic loads. This idea has a sense only in the case where response amplitude from dynamic loads is smaller than from the static action.

1. Introduction

In modern cities, transport needs are still increasing. Engineering objects like footbridges ensure a collision-free intersection of walking with roads, rail, and water routes. Their constructions are usually slim and visually light. This results from both visual trends and modern design possibilities. Footbridges, apart from their functional value, are also intended to attract attention or to become a characteristic element of the landscape. Due to the relatively low crowd load, footbridges do not require large, stiff cross-sections of structural elements. This is primarily because of the use of modern materials with high strength and increased capability and accuracy of design calculations, e.g., using Finite Element Method (FEM) in the design process [1–6]. This affects the implementation of spectacular projects characterized by unconventional static schemes, which happens when the designer, focusing on the form, does not notice the risk of the incorrect dynamic behavior of the footbridge in service. The best-known examples are the Millennium Bridge in London [7,8] and the Solferino Bridge in Paris [9,10]. It should be noted that excessive footbridge structure vibrations occur mainly under service load in the range of max. 20% of the ultimate value [11]. However, the vibration always must be reduced to the limit values specified by recommendations and standards.

In 2016, the construction of a drawbridge over the Motlawa River began in Gdansk. At the design stage, during the independent assessment, the footbridge (with a main span of 40.5 m) was subjected to numerical dynamic analysis. Unfortunately, natural frequencies in the critical range occurred. Moreover, due to architectural and mechanical reasons, there was no chance to change the span's geometry affecting the modal properties of the span. In this case, it was an opportunity to adapt the span driving mechanism to solve the problem of excessive bridge vibration. This paper shows the use of a driving hydraulic cylinder as a damper could reduce not only the vibration amplitudes but could also change the range of free vibrations.

Considering the equation of motion Eq. (1), the distribution of stiffness, damping, and mass has a significant impact on the dynamic

* Corresponding author.
E-mail addresses: krzysztof.zoltowski@pg.edu.pl (K. Zoltowski), annbanas@pg.edu.pl (A. Banas), mikbincz@pg.edu.pl (M. Binczyk), przkalit@pg.edu.pl (P. Kalitowski).

https://doi.org/10.1016/j.engstruct.2021.113781
Received 13 March 2021; Received in revised form 10 December 2021; Accepted 18 December 2021

behavior of the structure. Thanks to numerical simulations, it is possible to estimate the vibrations occurring in the service already at the design stage [12]. Thus, the first basic method of reducing footbridge vibration under pedestrian action is to modify the dynamic characteristics in the designing stage. When designing, an attempt should be made to shape the structure in such a way that the modal characteristics will not allow excessive vibration under pedestrian action. There are many cases where clever modifications of construction solutions can reduce or eliminate the potential problem of excessive vibration [12–14]. Of course, often available modifications to the structure do not bring significant changes to the modal parameters. In this case, only additional damping can solve the problem.

$$M\ddot{x}(t) + C\dot{x}(t) + Kx(t) = F(t) \tag{1}$$

Despite the continuous development of computational methods, due to the approximate nature of the simulation, designers often predict the possibility of the installation of external damping devices. Usually, the decision to install dampers depends on the results of the field test carried out after the construction process [15,16]. The purpose of the additional controlling devices is mainly to reduce the amplitude of vibrations to an acceptable level. There are many types of widely used damping devices. Due to the technology, we distinguish, among others: tuned mass dampers (TMDs) [17], tuned liquid column dampers (TLCDs) [18], viscous dampers [19,20], active tendons [21,22], and others. Thanks to their easy application, TMDs are the most commonly used and tested in many real cases [23–30]. They occur in single or multiple variants (MTMD) [31–34]. Due to the possibility of adapting to current conditions, the control devices are divided into passive, active, semi-active, and hybrid. Studies on a system developed in time involving various types of TMD devices are comprehensively presented in [35].

Both the numerical simulations of dynamic behavior at the design stage and the design of vibration reduction systems require knowledge of the modal characteristics of the structural system. These are sets of natural frequencies, forms, and damping. There are two general methods for determining the modal characteristics of structures: analytical and experimental. The first one usually employs a modal analysis performed on a numerical model [36–39], which can be done at the design stage but has limitations resulting from simplifying assumptions, mainly concerning damping, joint stiffness, and boundary conditions. On the other hand, the experimental method comprises conducting a field test to determine the modal characteristics of the real structure. For identification, controlled experiments are performed [40] and most often analyzed by experimental modal analysis (EMA) [41–45] or operational modal analysis (OMA) [46–50]. The main and obvious disadvantage of this method is the difficulty in an effective modification of the ready-made structure. Viscous dampers attached to the structure can change the dynamic characteristics of the system from proportional damping to nonproportional damping. This means that the modal parameters cannot be determined using the generalized or the standard eigenvalue problem implemented in commercial programs [51,52]. A clear description of this issue is presented, including an example, in [53]. [54,55] present various methods for determining the equivalent damping by adding viscous dampers. The theoretical analysis of the impact of viscous dampers used in buildings confirmed the phenomenon regarding the frequency and damping changes depending on the properties and location of the damper. Recommendations regarding the calculations of the impact of damper applications on the modal characteristics of the structure were also developed. [56] proved that viscous dampers can not only be used to dissipate energy but can also allow controlling the frequency of natural vibrations. The change in modal characteristics through the use of dampers is widely theoretically studied in seismic resistance of buildings [57–60]. The change in modal characteristics using dampers in the footbridge was mentioned in [1]. [61] describes the modeling methodology of structural systems supported by viscoelastic joints using of frequency response function coupling technique. [62] showed differences between various models of viscoelastic dampers used in theoretical analyzes. Viscous dampers are also used to change the vibration of tendons [63–65] or to reduce the amplitude of bridge span vibrations. Despite that, in the literature is a deficit of real examples showing the positive aspects of the phenomenon of changing the frequency of natural vibrations caused by the application of a viscous damper, with defined parameters, into the system. In the case of the described footbridge, an attempt was made to solve unconventionally the problem of critical natural frequencies. In the case of modern bascule bridges, driving hydraulic cylinders is a required element. They are used to open and close the passage. When the bridge is under pedestrian traffic, they are usually inactive.

This paper proposes a novelty use of a viscous damper to change a "static scheme" under dynamic load and reduce the excessive excitation of a footbridge. It was assumed that the use of the high damping unit will not only improve damping but also modify other modal characteristics to avoid critical natural frequencies. However, the solution does not affect the behavior of the structure under static loads. The required damping parameters were developed based on numerical calculations using FEM. Due to the nonproportional damping, the modal identification method was used to identify the equivalent modal characteristics. Finally, the solution was applied to the footbridge structure. The hydraulic system of the driving cylinder was modified to be a damper when the footbridge is opened to traffic. After construction, a field test was carried out to check the effectiveness of the solution and to evaluate the theoretical results. The paper is arranged as follows. In Section 2, the footbridge structure and the created numerical FEM models are described. Additionally, the theoretical basis of the system with the applied viscous damper, dynamic analysis, and modal analysis are presented. Then, Section 3 shows the validation of the simplified model developed for dynamic analysis, as well as the influence of the viscous damper on the footbridge's natural frequencies and accelerations. A field test conducted on the realized footbridge, consisting of modal identification, acceleration measurements, and testing of the move of the hydraulic cylinder, is described in Section 4. Subsequently, the results from the numerical analysis and the field test are compared and discussed in Section 5. Finally, conclusions are presented in Section 6.

2. Materials and methods

2.1. The simple theoretical model of the dynamic system with external damping

The analysis presented below does not correspond directly to the case study described in Section 2.2 but shows the phenomena of the developed idea. The general idea of the developed damping system is presented in Fig. 1, where k_1, k_2 denote internal stiffnesses, c_1 is internal damping, c_2 is external damping (driving cylinder) and m is a point mass. This simplified model shows how an external damper can change the basic dynamic properties of the system. The crucial element is a damper c_2. The system with assumed extreme values c_2 is presented in Fig. 2. If c_2 is very low (c_2 converges to zero), spring k_2 cannot act and the system is a standard one degree of freedom problem, where the stiffness equals:

$$k_{min} = k_1 \tag{2}$$

In turn, when c_2 is high (c_2 converges to infinity) displacement y_2 is quasi blocked and the system is again the standard one degree of freedom problem, where:

$$k_{max} = k_1 + k_2 \tag{3}$$

This means that the natural frequency of the system can be changed by modifying the c_2 value. General differential equations of motion for the system shown in Fig. 1 are given in Eq. (4). The solution of Eq. (4) was reached by numerical integration by using the Implicit Runge–Kutta method of the Radau IIA family of order 5, implemented

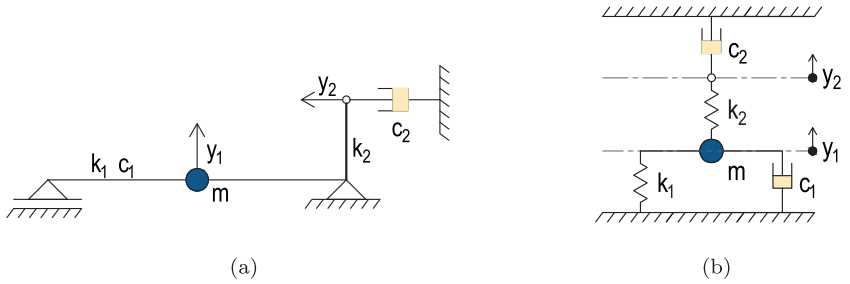

Fig. 1. Theoretical scheme of a considered dynamic system.

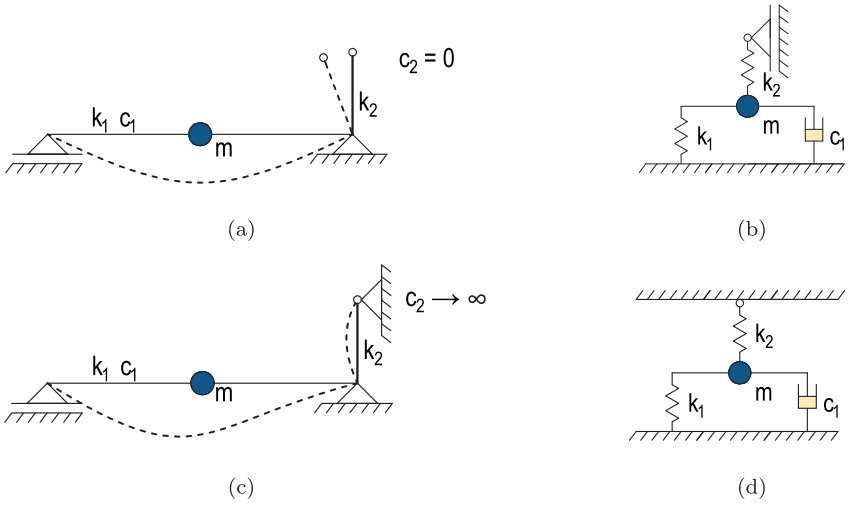

Fig. 2. Extreme cases of the theoretical system: (a), (b) c_2 converges to zero; (c), (d) c_2 converges to infinity.

Table 1
Constant and variable values of the system parameters used in the example solution (Fig. 3).

Symbol	m	k_1	k_2	c_1	c_2
Unit	[kg]	[N/m]	[N/m]	[Ns/m]	[Ns/m]
Value	1000	142,517	369,123	119	$10^1 - 10^7$

in the SciPy v1.4.1 Python package [66]. The resulting frequencies and logarithmic decrements of the signal y_1 for various c_2 are presented in Fig. 3. In an example solution, the constant values m, k_1, k_2, and c_1 and the variable c_2 were used. These values are gathered and exhibited in Table 1. The frequency f and logarithmic decrement δ were determined by analysis of the signal peaks. The verification of the numeric calculation of Eq. (4) was done by determining the limit frequencies, using the related stiffness k_{min} and k_{max} described by Eqs. (2) and (3). Based on the example stiffness values k_{min} and k_{max}, the limit frequencies equal $f_{min} = 1.900\,\text{Hz}$ and $f_{max} = 3.600\,\text{Hz}$, respectively. The limit frequencies are denoted as frequency asymptotes and marked in Fig. 3 by a horizontal dash–dot lines. Fig. 4 shows the natural response of the system (Fig. 1) excited by the initial displacement $y_1 = 1$ for three various values of damping c_2.

$$\begin{cases} m\ddot{y}_1 + c_1\dot{y}_1 + k_1 y_1 + k_2(y_1 - y_2) = 0 \\ c_2\dot{y}_2 + k_2(y_2 - y_1) = 0 \end{cases} \tag{4}$$

Summarizing the analysis presented above, particularly Fig. 3, we can formulate a simplified conclusion: changing a damping ratio c_2 from a small value to a critical range we can increase damping in system without significant change of natural frequency. Further increasing value of c_2 to "overcritical ratio" changes the stiffness of the system and changes the first natural frequency. This effect is accompanied by decreasing damping because c_2 does not act anymore as a damper in the vibrating system.

2.2. Structural overview

The footbridge in Old Town harbor in Gdansk, Poland, connects the Main Town with Olowianka Island (Fig. 5). It provides easier access to cultural objects in this part of the city, including the Baltic Philharmonic. It was decided to build a drawbridge because the Motlawa canal is navigable. The footbridge was built in 2017 and due to its location, in summer, the footbridge is opened every 30 min. The assumption for the footbridge design was that its height had to be relatively small and that it should not dominate the surroundings. Furthermore, it should not overwhelm the view of Old Town, but harmoniously inscribe in the historic landscape. The Slovenian company Ponting Inzynierski Biro developed the concept of the footbridge as part of an international competition. The final design was done by Mosty Gdansk. Modifications consisting in the introduction of additional damping were developed as part of the consulting work for the city by the team of Gdańsk University of Technology. The footbridge consists of a fixed part and a drawbridge. Fig. 6 shows the basic sections and a side view with the major dimensions and axes. The fixed part is a classical reinforced concrete 13.4-m-long span. The drawbridge part made of steel has a length of 40.5 m. The span has a variable geometry and consists of the main box girder in the middle of the cross-section and two 2.5 m carriageways. The deck was constructed as an orthotropic plate based on the cross-beams fixed to the main box girder (Fig. 6). The steel part was designed from structural steel S460N and S355N, while the reinforced superstructure from C30/37 concrete and the reinforcing steel A-III-N. On the bank of Olowianka Island, an abutment is integrated with the bridge's control room, where the hydraulic driving system, the control devices, and the service device are located. The span is lifted in the

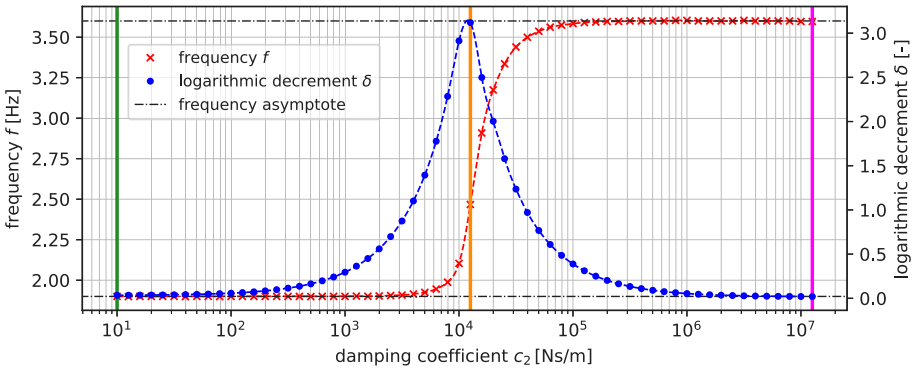

Fig. 3. The variation of natural frequency and the logarithmic decrement related to damper constant c_2, based on numerical solution of Eq. (4).

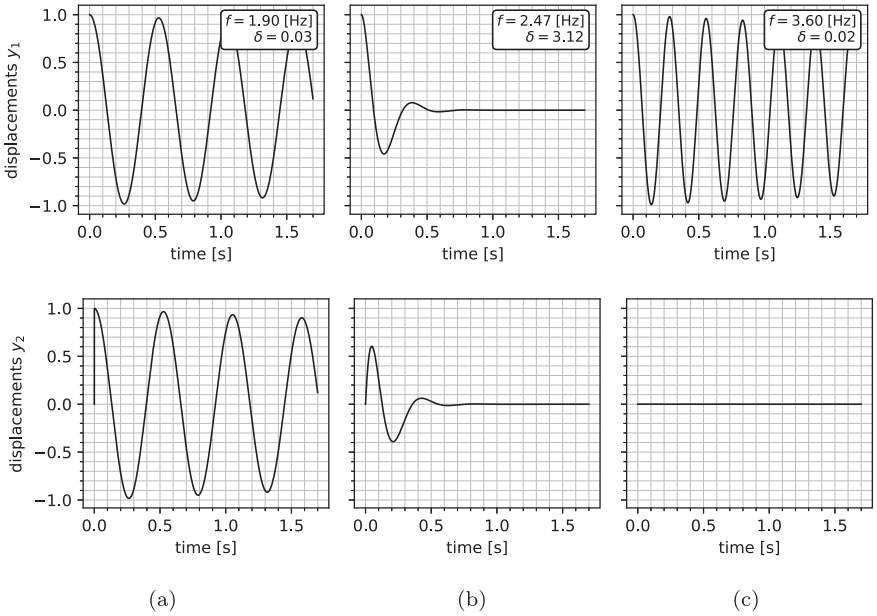

Fig. 4. Free response y_1 and y_2 of the system presented in Fig. 1 for (a) $c_2 = 10\,\text{Ns/m}$; (b) $c_2 = 12,589\,\text{Ns/m}$; (c) $c_2 = 12,589,254\,\text{Ns/m}$. The values (a), (b), (c) are denoted in Fig. 3 with vertical color lines: green, orange and magenta respectively.

Fig. 5. (a) Side view on the fully opened footbridge with its surroundings; (b) Side view of the footbridge from Olowianka Island; (c) Front view of the footbridge from the Main Town side.

range from 0° to 65° from the level by two hydraulic cylinders and then locked in the open position with a special locking device. When the bridge is in the closed position, the cylinders are inactive and the span is a simply supported beam (Fig. 7).

To apply the phenomena described in Section 2.1, Bosch Rexroth company, responsible for supplying the hydraulic system, was asked to implement an additional element in their design. This was a bypass between the working spaces of the double-acting hydraulic cylinder. The bypass was equipped with an electric valve and a manual reducer (Fig. 8). The bypass is closed by the electric valve during bridge rising operations (Fig. 7b) and it is opened when the bridge is used by pedestrians (Fig. 7a). The adjustment of manual reducer is permanent

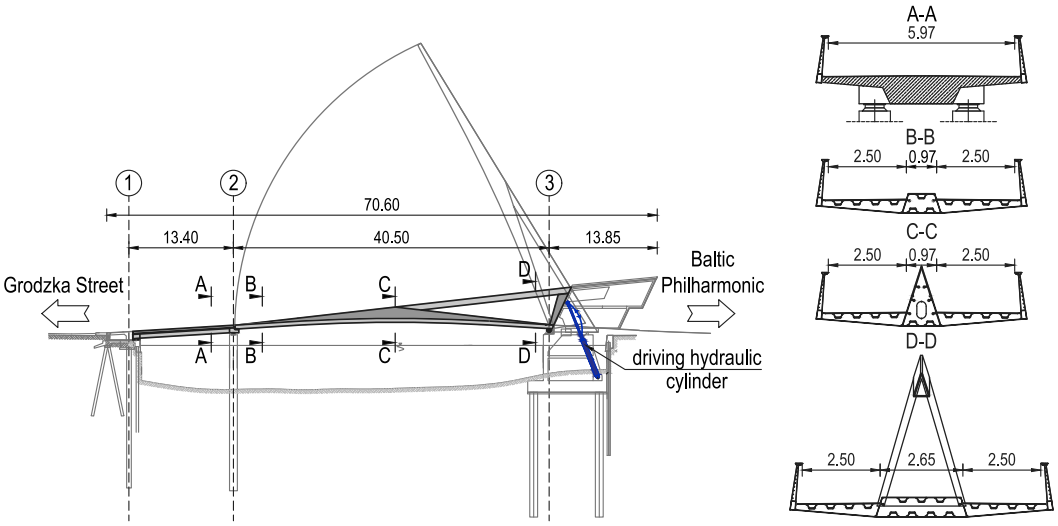

Fig. 6. Longitudinal view of the footbridge, the basic cross-sections, and the dimensions [m].

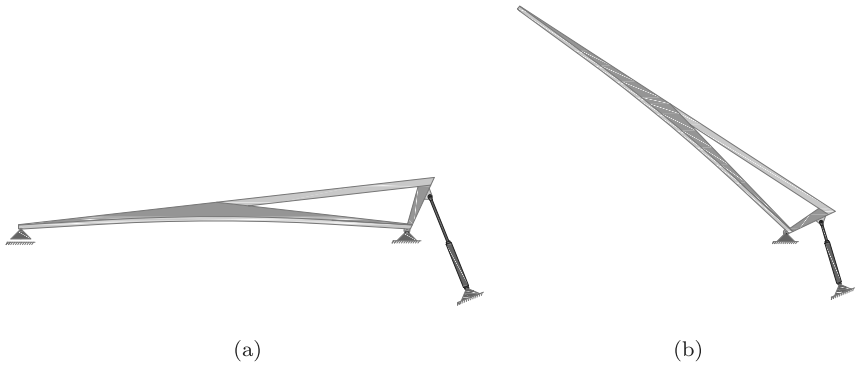

Fig. 7. Scheme of the footbridge with a driving cylinder: (a) in the closed position; (b) in the opened position.

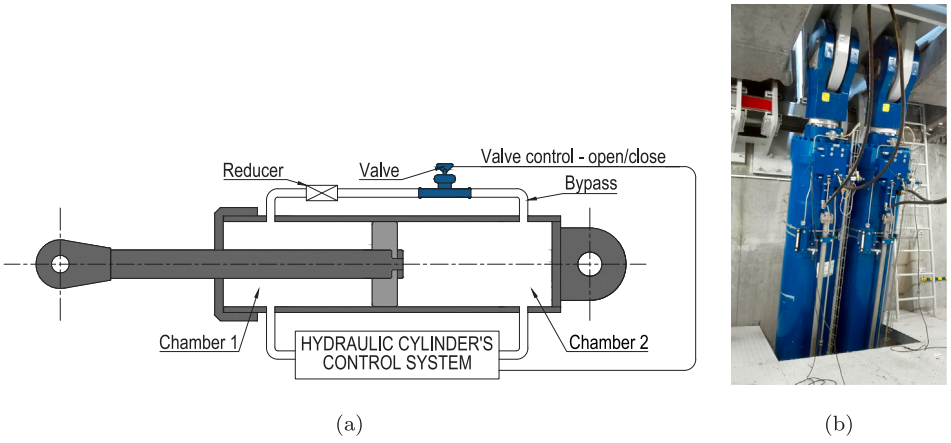

Fig. 8. A driving hydraulic cylinder: (a) a sketch of the hydraulic cylinder modification; (b) a real view of the driving hydraulic cylinders applied in the bascule bridge.

and was evaluated by Bosch Rexroth to fulfill designed damping requirements. As a result, hydraulic oil can flow between the working spaces of the cylinder when the drawbridge is lowered (Fig. 7a), thus the cylinder works as a damper. With added bypass, the hydraulic cylinder can be considered as a high ratio damper. This damper works only when the dynamic loads occur on the bridge. In the theoretical analysis, the linear damping law was assumed. The original design did not provide oil pressure in cylinder when the bridge is lowered.

2.3. Finite element model

At the design stage, the footbridge was subjected to numerical dynamic analysis. Because it is a time-consuming process, a FEM model should be simplified as much as possible, but should still be good enough to simulate a realistic dynamic response of the structure in the range interesting for a designer. In our case, two numerical models were made. The first one was composed of shell and beam finite

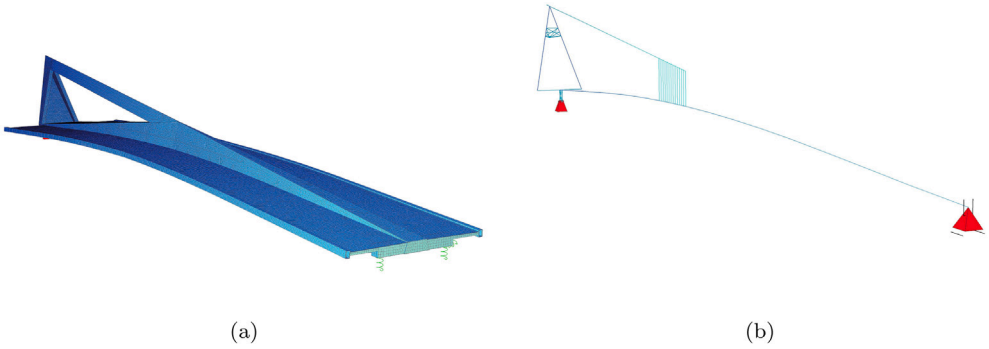

Fig. 9. Finite Element Method models: (a) the first one—shell and beam model; (b) the second one—beam model.

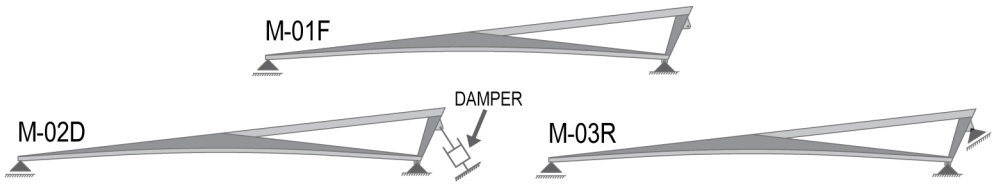

Fig. 10. The considered static schemes of the numerical models under operation.

elements (Fig. 9a). Shell elements are two-dimensional Timoshenko–Reissner-type quad-4 elements. These elements have an enriched state of deformation in the surface and reduction of the blocking effect. They also consider the shear effect and the different position of the coating reference surface (eccentricity). Beam elements are one-dimensional, two-node spatial finite elements of Timoshenko type. They take into account the shear effect and the eccentric beam axis. Most of the structure was modeled entirely from shell elements. Only the longitudinal ribs strengthening the main girder and the deck were modeled with beam elements. The second model was a beam model. In this variant, the model consisted of the main beam with variable cross-sections and additional beams that formed the triangular shape of the structure (Fig. 9b). The numerical models were made using commercial FEM SOFiSTiK software. In each model, the mesh convergence analysis was established in a few steps. At each step, the element size was reduced twice and the change in the structure's deformation was analyzed. When the change was not over 3%, the mesh convergence process was finished.

The complex and more precise first model was used to check the ultimate and serviceability limit states. The eigenforms and natural frequencies were also determined. The second beam model was validated by matching the dynamic modal characteristics and the static deflections under the test load to the shell–beam model. The structural mass (factor 1.03) and Young's modulus (factor 0.99) of the beam model were modified to obtain the same eigenforms, natural frequencies in the range up to 10 Hz, and static deflections. To investigate the potential effect of a supplementary viscous damper on the dynamic behavior of the footbridge, a beam (second) model was considered in the following three variants (Fig. 10):

- M-01F (Free model): The numerical model does not have any support point in the place of the driving cylinders.
- M-02D (Damping model): The numerical model has damping constraints in place and a direction consistent with the cylinders. Damper coefficient was initially set as $c = 3\text{E}4\,\text{kN s m}^{-1}$
- M-03R (Rigid model): The numerical model has rigid constraints in place and a direction consistent with the cylinders.

2.4. Dynamic numerical analysis

The first four eigenvalues (natural frequencies) were calculated for models M-01F and M-03R using the direct Lanczos method. The algorithm does not consider damping in the calculation of eigenvalues [54]. Thus, in the case of model M-02D, the determination of the natural frequencies was carried out by modal analysis of the free response of the structure. Free vibrations were computed as a response after the impulse forced near to the middle of the span. The Newmark direct integration method was applied for solving Eq. (1) based on Eq. (5) [67–69]:

$$\begin{aligned}\dot{\mathbf{x}}_{i+1} &= \dot{\mathbf{x}}_i + [(1-\gamma)\Delta t]\ddot{\mathbf{x}}_i + (\gamma\Delta t)\ddot{\mathbf{x}}_{i+1}\\ \mathbf{x}_{i+1} &= \mathbf{x}_i + (\Delta t)\dot{\mathbf{x}}_i + [(0.5-\beta)(\Delta t)^2]\ddot{\mathbf{x}}_i + [\beta(\Delta t)^2]\ddot{\mathbf{x}}_{i+1}\end{aligned} \tag{5}$$

where i is a step number; the integration step was established as $\Delta t = 0.01$ s; and the control parameters of the method γ and β were established according to the original Newmark method as $\gamma = 1/2$ and $\beta = 1/4$. This ensures a calculation without additional numerical damping. The free response was tested at several points of the model, and then a Fast Fourier Transform (FFT) was performed on the obtained vibration signals to identify the natural frequencies. Compared to the eigenvalues, these frequencies consider the influence of a high dumping element in the system. Based on these, a preliminary assessment of the pedestrian bridge's sensitivity to dynamic loads can be made. When the natural frequency is about 2.0 Hz, a comprehensive dynamic analysis must be performed [11,13,23]. For a further detailed analysis of the dynamic response of the footbridge, the three numerical models described above (Fig. 10) were carried out under the following loads defined in [12]:

- L-01Part—the pedestrian stream partially synchronized.
- L-02Full—the pedestrian stream fully synchronized.
- L-03V—squats performed by a group of people (vandalistic load).

In all load models, the excitation frequency was adjusted to the first natural frequency, which is different in the three considered numerical models. Fig. 11 shows an exemplary excitation with an amplitude frequency of 2.0 Hz.

The first load (L-01Part) is a load case representing pedestrians walking on the footbridge. Studies carried out by [71] and confirmed by [12] indicate that statistically, the number of synchronized pedestrians is equal to the square root of the number of all pedestrians. The

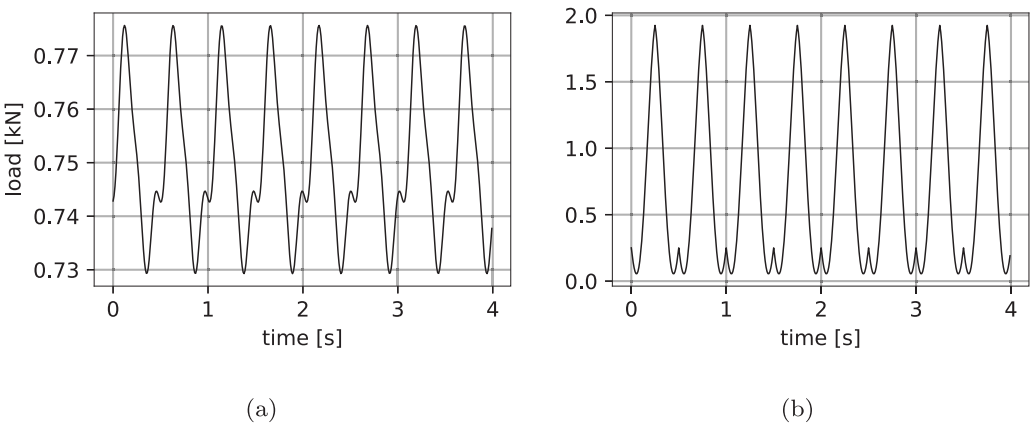

Fig. 11. Example models of pedestrian load developed in [12,70]: (a) single pedestrian walking; (b) squats of single pedestrian.

load from a single pedestrian (Fig. 11a.) was multiplied by the number of synchronized pedestrians. The second load case (L-02Full) is similar to L-01Part; however, in this load, all pedestrians are synchronized. The last load (L-03V) is a vandalistic load case. It comprises purposeful squatting on the footbridge, which is supposed to cause big vibrations. In this case, the load frequency is fully synchronized with the natural frequency of the bridge. The impact of squatting by a single pedestrian (Fig. 11b.) was, in this case, multiplied by the number of squatting pedestrians. It was assumed that the squats would be performed by a group of 20 people. Analysis of the dynamic response of the load cases was performed using the Newmark time step method with classical proportional structural damping applied according to Rayleigh (Eq. (6)) [68].

$$\mathbf{C} = \alpha_1 \mathbf{M} + \alpha_2 \mathbf{K} \tag{6}$$

Proportionality coefficients α_1 and α_2 were selected to provide a logarithmic decrement of about 2.4% [15]. For determination of the coefficients, Eq. (7) was used. In the formula, it is assumed that for both modes ω_i and ω_j, the same damping ratio ξ is adopted, which is reasonable based on experience and experimental data.

$$\alpha_1 = \xi \frac{2\omega_i \omega_j}{\omega_i + \omega_j} \qquad \alpha_2 = \xi \frac{2}{\omega_i + \omega_j} \tag{7}$$

2.5. Modal analysis

Modal analysis is a method used to identify the dynamic properties of the structure. One can distinguish methods based on the measuring and processing of input and output data, or output data only. Among the methods based on output data only, it is the simplest use of a free vibration signal. In a numerical and field dynamic test of a footbridge, there is usually no problem in exciting free vibrations and measuring time-domain free-decay displacements or accelerations. There exist numerous techniques for identifying the modal parameters from free vibration signals [72,73]. In this case, the ERA (Eigensystem Realization Algorithm) was adopted [74–77], which is an efficient and popular time-domain method of modal parameter identification, confirmed in many civil engineering applications. The ERA is related to control theory and utilizes state-space representation of a discrete-time, linear, time-invariant system in the form of Eq. (8):

$$\begin{aligned} \mathbf{x}(k+1) &= \mathbf{A}\mathbf{x}(k) + \mathbf{B}\mathbf{u}(k) \\ \mathbf{y}(k) &= \mathbf{C}\mathbf{x}(k) + \mathbf{D}\mathbf{u}(k) \end{aligned} \tag{8}$$

where $\mathbf{x}(k)$ is the vector of the states; $\mathbf{u}(k)$ is the vector of the system inputs; $\mathbf{y}(k)$ is the vector of the system outputs at the kth step; $\mathbf{A}, \mathbf{B}, \mathbf{C}, \mathbf{D}$ are the discrete-time state-space matrices; and the order of the model is the number of components of the state vector $\mathbf{x}$. The ERA is a method based on Markov parameters (i.e., free-decay vibrations). In the first step, the Hankel matrix is formulated from the Markov parameters. The second step is a factorization of the Hankel matrix using Singular Value Decomposition (SVD). Due to the existence of noise in the acquired data, a minimal realization is obtained by eliminating relatively small singular values in the matrices resulting from the SVD. Subsequently, the estimated system matrices that are minimal realization can be calculated. After that, the eigenvectors and the eigenvalues can be found by solving the eigenvalue problem using the obtained estimated system matrices. Before calculation of the modal parameters, a discrete-time system must be transformed to the corresponding continuous-time system. The modal damping rates and the damped natural frequencies can be obtained from the real and imaginary parts of the eigenvalue matrix. In turn, the mode shapes can be calculated using the eigenvector matrix.

In the ERA, assuming the model order is a crucial aspect. Thus, to evaluate the assumed model order, a stabilization diagram is created. To determine the diagram, the identification process is repeated with different (increasing) model orders. If the modes are stable, they should remain constant in most iterations. Additionally, a filtered version of the stabilization diagram can be generated [78], which is created using the criteria of the evaluation of the solution modes. In presented work, MAC (Modal Assurance Criterion [79]) and MPC (Modal Phase Collinearity [80]) were employed.

3. Numerical results

3.1. The dynamic characteristics and beam model validation

An eigenvalue analysis was performed for the numerical shell–beam model. The first four forms of natural vibration were determined together with the corresponding vibration frequencies. The results of the eigenproblem are presented in Fig. 12a–d, which shows that the footbridge is characterized by a low frequency of vertical natural vibrations (1.64 Hz) in the critical range below 2 Hz. The beam model was validated by matching the dynamic characteristics and stiffness with the shell–beam model. The achieved forms and frequencies of the beam model are alike those of the shell–beam model (Fig. 12e–h). The diagrams shown in Fig. 12 do not include additional support in place of the hydraulic cylinders. The first natural frequency is exactly 1.64 Hz for both the shell and beam model. The validated beam model was used for further numerical dynamic analysis.

Table 2 shows a comparison of the determined natural frequencies for the beam models M-01F, M-02D, and M-03R (Fig. 10). The analysis of the free response of the structure after an impulse forced in the middle of the span was performed with the Newmark time-step method. Fig. 13 presents the received signals and their FFT analysis results are presented in Fig. 14. The dominant vibration frequencies determined for model M-02D with the damper coefficient c = 3E4 kN s m^{-1} are

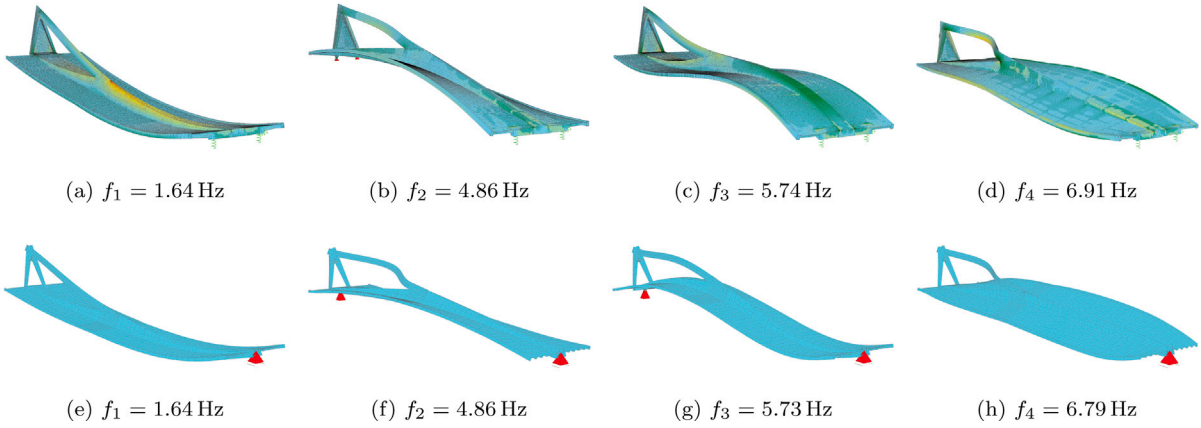

Fig. 12. Comparison of first four eigenforms and eigenfrequencies: (a–d) Shell-beam FEM model; (e–h) beam FEM model.

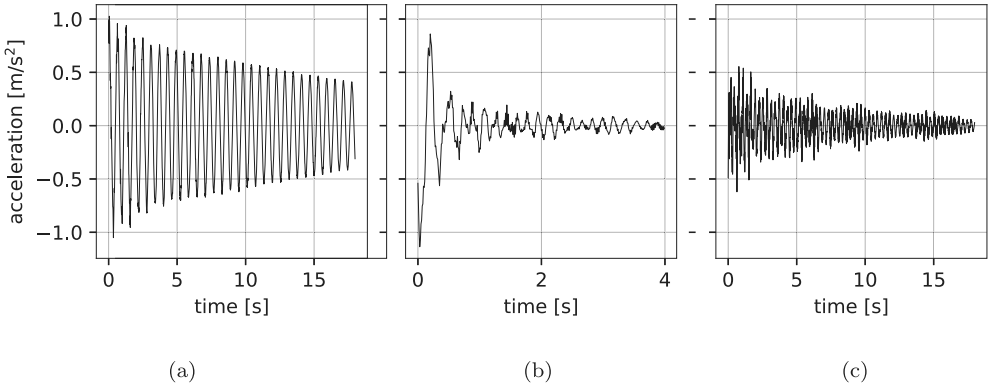

Fig. 13. Comparison of the free response accelerations for the numerical models: (a) M-01F, (b) M-02D (c = 3E4 kN s m^{-1}), and (c) M-03R.

Table 2
Comparison of the natural frequencies for the different variants of the FEM beam model (Fig. 10).

Eigenform	Natural frequencies [Hz]		
	M-01F	M-02D	M-03R
First bending form	1.64	3.13	3.38
First torsion form	4.86	4.86	4.86
Second bending form	5.73	5.85	5.89
Second torsion form	6.79	6.79	6.79

close to the natural frequency obtained for the model M-03R (Table 2). This means that cylinders with such high damping are "almost" rigid support for the span, and the first dominant natural frequency goes beyond the area critical for footbridges. It should be noted that this rigid support effect is only achieved for dynamic loads. For static and quasi-static (long-term) loads, there is no force in the damper, and the static diagram for long-term loads is a freely supported beam, as in the M-01F model. Despite such satisfactory natural frequencies for the model M-02D, it was conducted a detailed analysis of the dynamic response of the footbridge for all three variants of the numerical models.

3.2. Influence of the viscous damper on the footbridge

Based on the phenomenon presented in Section 2.1, the influence of the defined viscous damper (driving hydraulic cylinders) on the dynamic behavior of the designed footbridge was studied. The simplified model M-02D was used in the calculation. Initially, a small damper constant was considered and dynamic analysis was performed to get the free response of the footbridge. A small damper constant ensures, in the first iteration, no significant effect on the frequency and damping of the structure. The obtained signal was analyzed using the ERA algorithm. The natural frequencies and modal damping were identified for the first four modes. Subsequently, the damper constant was increased and dynamic and modal analyzes were performed. Increasing the damper constant, these steps were repeated to get the frequency and modal damping relationship shown in Fig. 15. The results are presented for vertical bending forms 1 and 3 (Fig. 12) only. No effect on torsional forms 2 and 4 (Fig. 12) was observed. This is due to the location of the hydraulic cylinder and the lack of its influence on torsional vibrations. The frequency asymptotes for each mode are marked with horizontal lines on the charts, and they show the natural frequencies obtained using the M-01F (lower) and M-02R (upper) models. It can be seen that the damper constant changes the natural frequency values in the range of borderline cases, from free to rigid support. Analyzing the relationship between modal damping and the frequency, it can be seen that the maximum damping occurs near to the frequency curve's inflexion point. At the design stage of the footbridge, the principal objective was to raise the frequency of natural vibrations as far from the critical range as possible. Hence, the minimum damper constant c was chosen, where the frequency is close to the upper asymptote with the minimum value of c simultaneously. This value, c_e = 3E4 kN s m^{-1}, is marked in Fig. 15 by a vertical black line. It is assumed that any value of the damper constant greater than c_e is considered as acceptable if the accelerations from the pedestrian loads meet the comfort conditions. The results of the dynamic analysis are presented in Section 3.3; the condition is met and the determined value of c_e was delivered to the contractor of the hydraulic cylinders, with an indication that the resulting damper constant of the modified hydraulic cylinders cannot be smaller than the value of c_e.

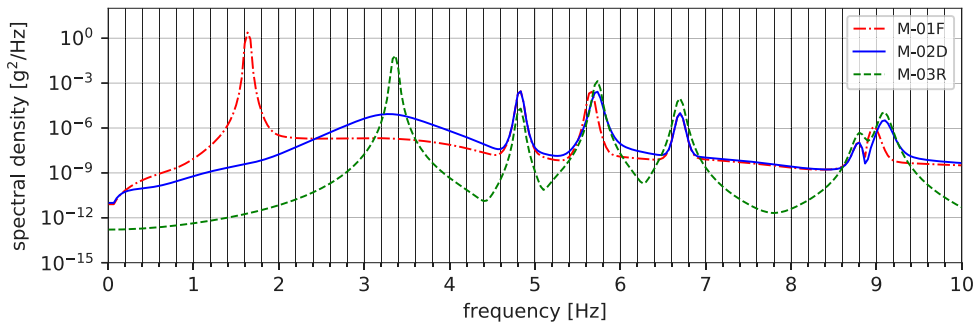

Fig. 14. Fast Fourier Transform (FFT) analysis of the free response accelerations calculated by the FEM beam models.

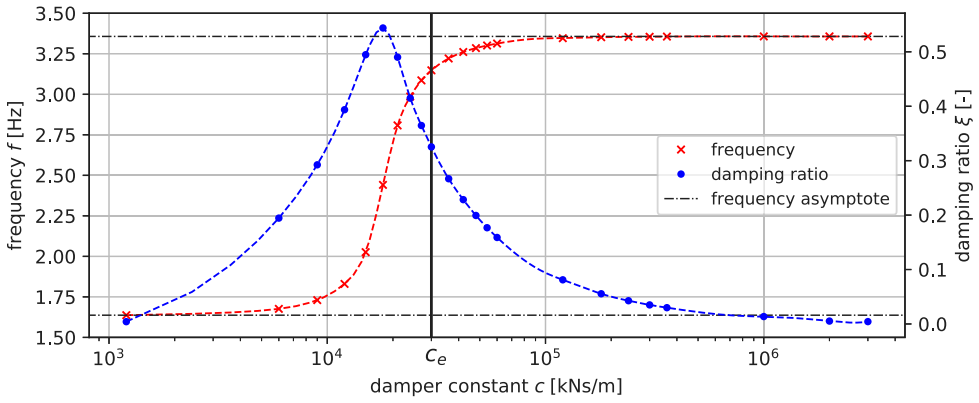

(a)

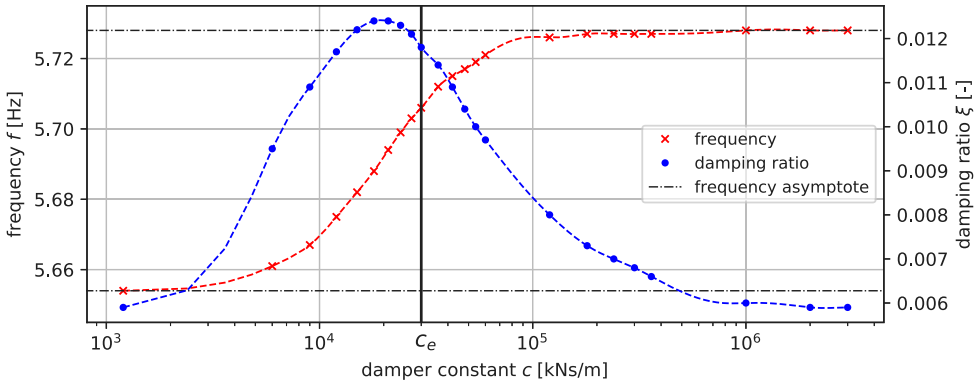

(b)

Fig. 15. The modal damping and natural frequency vs. the damper constant for the numerical model M-02D: (a) 1st mod, (b) 3rd mod.

3.3. Pedestrian loadings

The response of the footbridge under pedestrian action was estimated using the time-step method with the Newmark algorithm in SOFiSTiK software. The structural responses under loads L-01Part, L-01Full, and L-03V were calculated. Fig. 16 presents graphs comparing the obtained vertical accelerations in the middle of the bridge span depending on the model variant got for a partially synchronized pedestrian stream (load L-01Part). Additionally, Fig. 17 shows the results for the L-03V load case. Table 3 presents the results of the maximum displacements and accelerations obtained for the three numerical models (M-01F, M-02D, and M-03R) and the three load models. If the damper is included in the analyzes (M-02D and M-03R), the amplitude of the vibrations is much lower compared to the model without the damper (M-01F).

The comfort classes are defined in [81] and presented in Table 4. Based on this and the results of the dynamic analysis (Table 3) for the model M-02D under load L-01Part, it was determined that the footbridge with the use of hydraulic cylinders as dampers would ensure a high level of comfort (class K1). The load case L-02Full (dynamic acting of pedestrian flow, fully synchronized, filling 100% of the deck) is an unlikely situation. However, if it occurs, the footbridge will provide users with a minimum level of comfort (class K3). In the case of vandalistic loads (L-03V), the comfort criterion is not considered but the load capacity criterion is. It is assumed that vandalism will not be disturbed by excessive vibrations of the bridge. Here, the safety condition of the structure must be respected. The results for this load

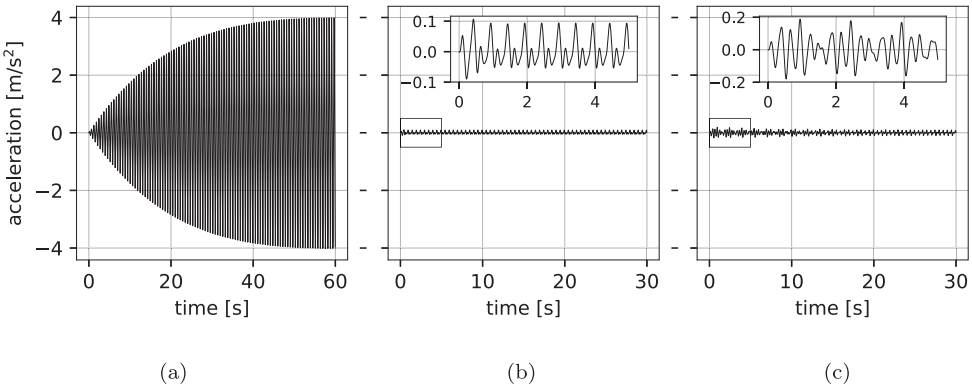

Fig. 16. Graphs of vertical acceleration for a partially synchronized pedestrian stream (L-01Part) with the excitation frequency f_e: (a) M-01F $f_e = 1.64$ Hz; (b) M-02D $f_e = 3.13$ Hz; and (c) M-03R $f_e = 3.38$ Hz.

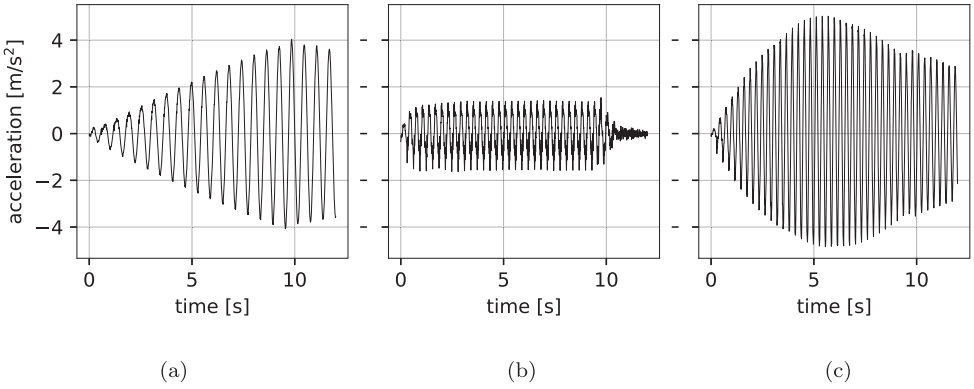

Fig. 17. Graphs of vertical acceleration for squats performed by twenty people (L-03V) with the excitation frequency f_e: (a) M-01F $f_e = 1.64$ Hz; (b) M-02D $f_e = 3.13$ Hz; (c) M-03R $f_e = 3.38$ Hz.

Table 3
Summary results of dynamic analysis.

Load	Value	FEM model acc. Fig. 9		
		M-01F	M-02D	M-03R
L-01Part	dz [mm]	36.93	0.35	0.46
	az [m s^{-2}]	3.91	0.11	0.19
L-02Full	dz [mm]	69.08	5.33	6.85
	az [m s^{-2}]	3.92	1.62	2.85
L-03V	dz [mm]	37.38	1.44	10.43
	az [m s^{-2}]	4.04	0.91	5.03

Table 4
Comfort classes for footbridges by [81].

Comfort class	Level of comfort	Vertical acceleration
		[m s^{-2}]
K1	High	Less than 0.5
K2	Medium	0.5÷1.0
K3	Minimal	1.0÷2.5
K4	Unacceptable	More than 2.5

case indicate very small displacements of the deck—only 1.44 mm, which is a very small value compared to the deflection from a static load required by the standard. It is worth noting that when there is no damper (model M-01F), the level of comfort is unacceptable. Dynamic footbridge response analysis was also performed for a damper constant higher than the recommended value ($c > c_e$). The maximum accelerations obtained for the L-01Part load depending on the adopted damper constant are shown in Fig. 18. It should be noted that the comfort level is still the highest for each $c > c_e$.

4. Field test

The footbridge tests were carried out during a test load before being opened to service. They took place on June 17, 2017, and comprised static and dynamic tests. The tests were carried out late in the evening and at night to dispose of the effects of temperature changes associated with sun operation on the obtained static results. The tests were carried out by the Field Research Laboratory, which is part of the Department of Railway Transportation and Bridges of the Gdansk University of Technology.

During the static field tests, the maximal vertical displacements, the settlement of the supports, and the vertical deformations of the bearings were measured. As the static load, 43 water tanks with a unit weight of 10.5 kN were used (Fig. 19). The maximum measured elastic displacement in the middle of the span was 71.2 mm. Corresponding theoretical displacements obtained for the M-01F model were 76.6 mm. The measured value is 93% of the theoretical displacements. Differences between the theoretical and real displacements are due to measurement errors, the value of the real test load, a real redistribution of structure stiffness, and a disregarding of railings in the numerical model. It should be mentioned that the theoretical model was built on the design stage and was not calibrated, thus received error is acceptable. On the other hand, if we assume the infinite stiffness in the cylinder's place (M-03R model - blocked oil pressure in the cylinder), the static displacement would be only 16.1 mm. The static test load confirmed that the footbridge works as a simply supported beam for static loads.

During the dynamic tests, the platform's accelerations were measured at eight measuring points; the vertical accelerations were measured at six points and the horizontal acceleration at two points. Vertical accelerometers were located at 1/4, 1/2, and 3/4 of the span length.

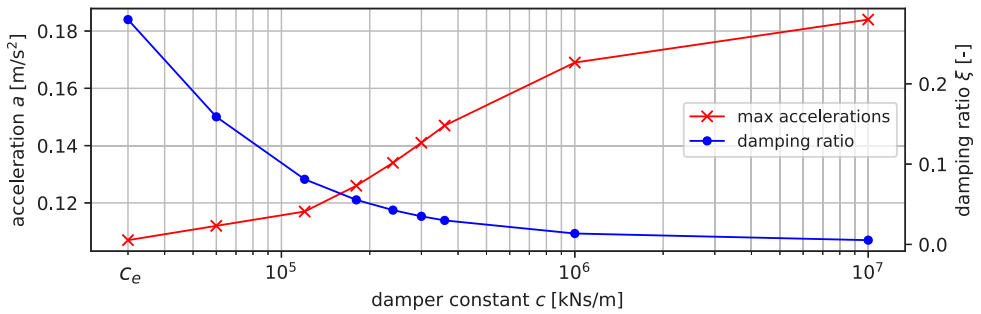

Fig. 18. The relation between the damping ratio ξ, the maximal acceleration of the span a, and the damper constant c under a partially-synchronized march. The results are limited to the recommended values of c higher than c_e (p. 3.2).

Fig. 19. The static load during the field test: (a) side view with the measurement point marked; (b) the water tanks during the field test.

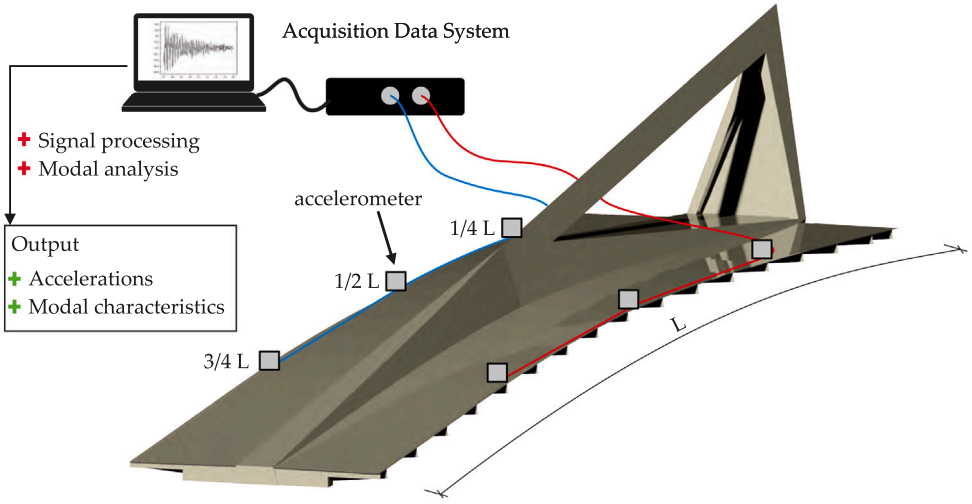

Fig. 20. Dynamic measurement scheme.

The arrangement of the measuring points is shown in Fig. 21a. Three-axial micro-electro-mechanical capacitive accelerometers (MEMS) of the LIS344ALH type manufactured by STMicroelectronics (Geneva, Switzerland) (Fig. 21b) were used to measure the structure's vibration response. Measurement data were recorded using the QUANTUM HBM 840a (Hottinger Baldwin Messtechnik GmbH, Darmstadt, Germany) eight-channel measurement amplifier (Fig. 21b). The measuring stand (Fig. 20) also consisted of a laptop used for data processing, visualization, and storage of measurement results.

4.1. Dynamic tests

The main loads on the footbridge are walking and cycling people, but due to its location in the city center, there is an incidental risk of vandalistic loading of the footbridge. Therefore, it was carried out a wide range of dynamic tests and to identify and verify the dynamic behavior of the footbridge under various dynamic loads. The performed tests included the following excitations: synchronous and free march, synchronous and free running, as well as squatting of a group of twenty pedestrians (Fig. 22). At first, to synchronize the applied pedestrian excitation with a resonant frequency, the dynamic parameters of the footbridge were identified by analyzing the free response. Free vibrations were induced with impulsive jumping of a group of 20 people. Based on the Fast Fourier Transform (FFT) analysis of the vertical acceleration signal measured in the middle of the span, the natural frequencies of the footbridge were identified in the field. The main frequency was 3.1 Hz, which is close to the first natural frequency developed in the numerical analysis; thus, it was assumed as the first

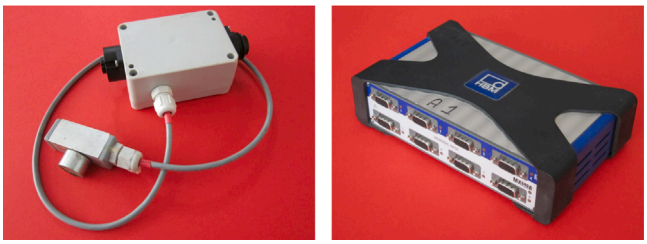

(a) (b)

Fig. 21. (a) Tri-axial micro-electro-mechanical capacitive accelerometers (MEMS) accelerometer; (b) QUANTUM HBM 840a eight-channel measurement amplifier.

Table 5
The natural frequencies and modal damping ratios identified in the field test.

Mod	1	2	3	4
Frequency [Hz]	3.098	4.357	5.723	6.921
Damping ratio [–]	0.0343	0.0027	0.0056	0.0057

Table 6
Summary results of the maximum vertical accelerations from the field test of human-induced vibrations.

Type of human-induced vibration	Free march	Synchronous march	Free running	Synchronous running	Synchronous squatting
Maximum acceleration [m s^{-2}]	0.22	1.83	0.8	2.33	3.08

bending form of the structure. Therefore, further tests were carried out with the frequency 3.1 Hz and additionally with a frequency close to the standard human step of 1.9 Hz. Three measurement series were performed for each type of excitation.

The modal analysis was performed using the ERA algorithm. To identify the modal parameters, the free response signals from six vertical accelerometers were used. Before analysis, the signals were processed. To limit the range of the resulting model poles to 15 Hz, the signals were downsampled to 30 Hz. The method's parameters were established iteratively to get the stable modes occurring on the stabilization diagrams. The nonfiltered version of the final diagram is presented in Fig. 23a; in turn, the filtered version is shown in Fig. 23a. As in the numerical model, four mods occurred in the range from 0 to 8 Hz. For each of them, the natural frequency, the damping ratio, and the form of vibration were calculated. The identified frequencies and damping ratios are concluded in Table 5. Fig. 24 presents the identified form, where the measured points are marked with green dots; they are also projected onto the $z = 0$ plane with red dots, and the black dots are fixed points. For the spatial presentation of the forms, a cubic spline was drawn through the black and green dots. Generally, it can be seen that the first four mods in comparison with the numerical modal shapes have similar forms, which allows comparing the respective natural frequencies between the field and numerical results.

An important aspect of the research was checking the comfort of pedestrians moving along the footbridge. The measured acceleration signals were used to evaluate comfort, and all recorded signals were processed. The trend line was removed and then they were filtered. A 5th Butterworth band-pass filter was used, which allowed filtering the components with frequencies below 0.5 Hz and above 10 Hz from the signal, as they were outside of the area of interest. Fig. 25 presents the example time histories of the vertical accelerations of the deck acquired in the middle of the span. In Fig. 25a, the response under a free walk is shown; in turn, in Fig. 25b, the accelerations under synchronized squatting are demonstrated. Table 6 summarizes the maximum acceleration values of the footbridge structure under each type of excitation.

Table 7
Summary results of the theoretic and measured values of natural frequencies of the span.

Eigenform	Natural frequencies FEM [Hz]			Field test [Hz]
	M-01F	M-02D	M-03R	Real structure
First bending form	1.64	3.13	3.38	3.098
First torsion form	4.86	4.86	4.86	4.357
Second bending form	5.73	5.85	5.89	5.723
Second torsion form	6.79	6.79	6.79	6.921

5. Discussion

Damping ratios are one of the most important factors that influence the prediction of footbridge dynamic behavior. However, they are one of the most difficult parameters to estimate in the design stage. It is important not to overestimate structural damping to ensure a conservative prediction of vibration in service, especially if there is a risk of resonance associated with humans walking on the footbridge. In this case, it is advisable to design additional damping devices. However, the prediction of the dynamic behavior of the footbridge with an applied damping system is even more complicated and should be supported by comprehensive research.

The final dynamic parameters of the footbridge were identified based on the field test, and confirmation of the theoretical assumptions was carried out. Table 7 presents the comparisons of the natural frequencies obtained during the field test and the previous numerical analyzes. Generally, the values are similar. Moreover, the eigenforms identified in the field test for each mod have the same shape as in the numerical model, as can be seen in the comparison of Figs. 12 and 24. However, there are differences between the natural frequencies, which can be caused by several issues. The results presented in Table 7 compare the design stage and the state obtained after construction. The identified first natural frequency is 3.098 Hz which is 99% of the theoretical value. Despite the lack of final calibration, they show high compatibility. The differences in the results are due to the same reasons as in the static analysis (Section 4). Dynamic analysis is an even more complex issue because of the necessity of considering the structural mass distribution and damping. At the design stage, two important parameters were theoretically predicted: the structural damping of the bridge structure and a damping coefficient of a hydraulic cylinder. Confirmation of the structural damping of the bridge should be done under construction when the span was not connected with driving cylinders. Unfortunately, this moment was missed because of the construction process. Furthermore, the identification of the real value of the external damper coefficient was theoretically possible but also missed during the construction process. The theoretic damping coefficient of cylinder $c = 3E4$ kN s m^{-1} was considered in the design stage. According to the further analysis, as shown in Fig. 15, this value can be taken as the minimum.

However, one can consider the following case: is it possible that such a big cylinder, with adopted such high damping coefficient, is completely blocked and insensitive to a relatively small dynamic load. In that case, it would work as a rigid support. To confirm the cylinder works even under the small dynamic load, an additional test was conducted (Fig. 26). Displacements between the cylinder tube and the piston rod were measured under the dynamic excitation. The inductive displacements' sensor was installed between those two parts (Fig. 26b). As a dynamic test load, a group of four people tried to excite structure with the first natural frequency. The result of piston movement is shown on Fig. 26a. Maximum obtained amplitude is c.a. 0.008 mm. Theoretically, with absolutely no damping in the cylinder, the displacement in the direction of the piston under the test load should be 0.185 mm (according to the FEM analysis - model M-01F). It allows us to conclude that the hydraulic cylinder is acting dynamically even under a relatively small dynamic load, but the effect of the high damping may provide behavior close to the rigid support.

(a) (b) (c)

Fig. 22. Dynamic tests performed on the footbridge: (a) synchronous march, (b) synchronous and free running, as well as (c) squatting of groups of twenty pedestrians.

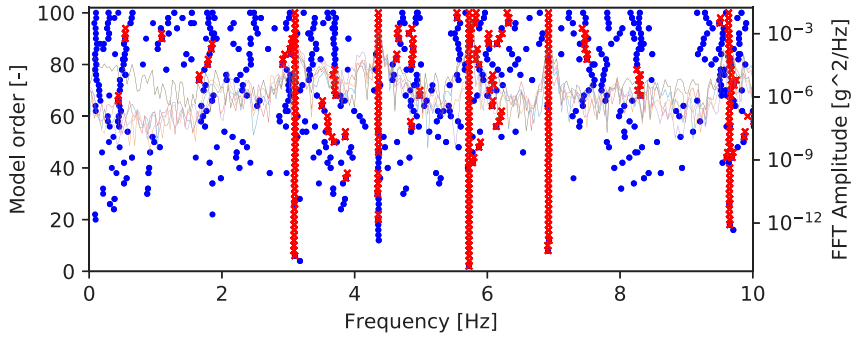

(a)

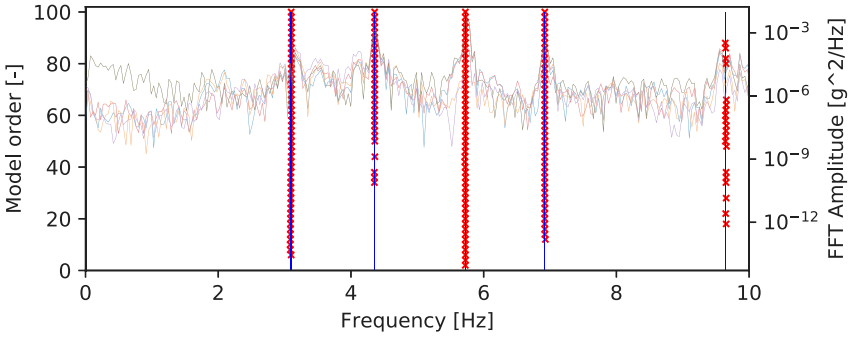

(b)

Fig. 23. Stabilization diagrams of the Eigensystem Realization Algorithm (ERA) method: (a) Non-filtered version; (b) filtered version.

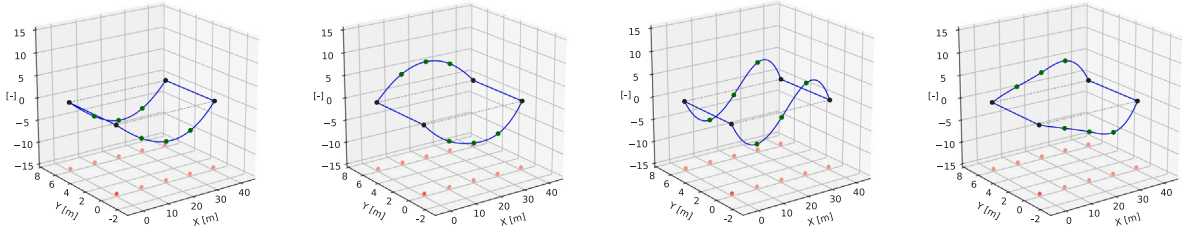

(a) (b) (c) (d)

Fig. 24. First four eigenforms of the footbridge identified in the field test (a) 1st mod, (b) 2nd mod, (c) 3rd mod, (d) 4th mod. (For interpretation of the references to colour in this figure legend, the reader is referred to the web version of this article.)

Based on the field research and numerical calculations, the acceleration time histories of the structure at selected measuring points were obtained. Fig. 27 shows the representative acceleration time histories during free walking and squatting got from the field tests and the

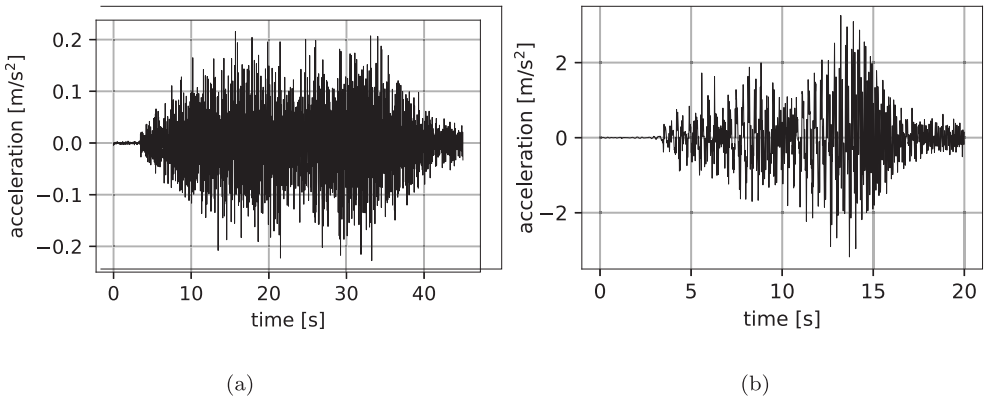

Fig. 25. Representative time histories of vertical acceleration in the middle of the footbridge under (a) a free march and (b) synchronous squatting.

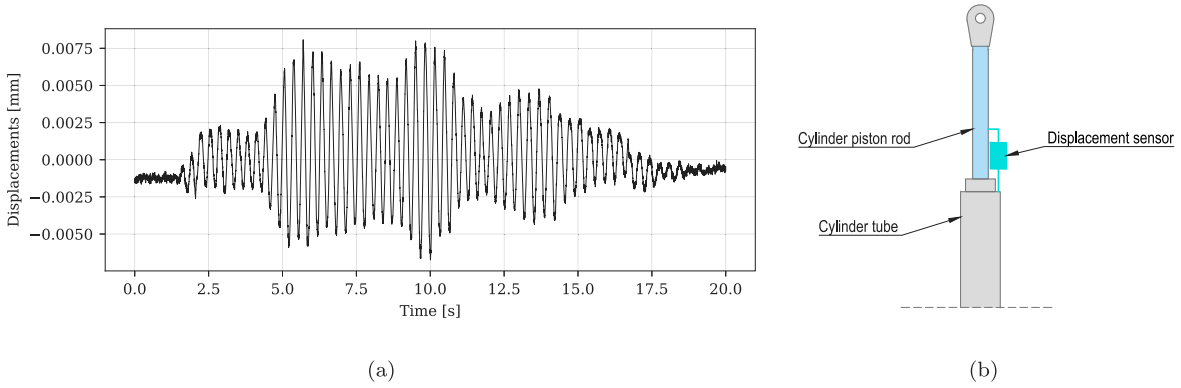

Fig. 26. The field test of the dynamic work of the hydraulic cylinder: (a) measured displacements between the piston rod and the cylinder tube under the dynamic load; (b) the scheme of the sensor location; (c) the inductive sensor (not finally connected).

Table 8
Summary results of the experimental and analytical class comfort for the footbridge.

Load	Max acceleration [m s^{-2}]		Comfort class
	Field test	FEM model M-02D	
L-01Part	0.19	0.14	K1
L-02Full	1.83	2.26	K3
L-03V	3.08	2.99	K4

numerical calculations (model M-02D). The maximum accelerations calculated by the FEM model, measured in the field test and the corresponding expected comfort levels are presented in Table 8. It was found that the footbridge provides a high level of comfort under normal exploitation conditions. The maximum acceleration values under free walking correspond to the first comfort class and are significantly lower than 0.5 m s^{-2}. The maximum acceleration values under fully synchronized walking, with the pacing rate corresponding to the first vertical natural frequency of the span, fulfill comfort criteria for class three (maximum reached acceleration was 1.83 m s^{-2}). A different situation occurs during intentional pedestrian excitation at a particular frequency in the middle of the span. Here, the vibrations oscillate at the level of the minimum acceptable vibration level (up to 2.5 m s^{-2}). Such excitation should be considered as an intentional vandalistic action, which cannot be treated as normal exploitation. Therefore, it is not required to fulfill the comfort criteria.

The presented frequencies (Table 7) and the predicted response in Fig. 27 confirm the compliance of the proposed FEM model with the real structure. The analysis of the influence of the appropriate damper constant allowed us to build a footbridge that fulfills the comfort criteria. Supposedly, in the case of a footbridge not equipped with an additional damping device, there is a risk of excessive vibration during the exploitation. This is shown in Table 3, which compares the maximum accelerations for the three models: the model without additional support (M-01F), the model with an additional damping device (M-02D), and the model with rigid support (M-03R) in place of the driving hydraulic cylinder. There is a significant reduction in the accelerations of the M-02D model compared to the M-01F and M-03R models, which can be considered, along with the high compliance with field tests, as a confirmation of the assumptions regarding the impact of a viscous damper on the structure. Application of the damper supported by the conducted analysis allowed not only to reduce the value of the acceleration but to shift primarily the natural frequency outside of the range directly related to walking as well. The presented results confirm the correct selection of the damper constant and the entire process of dynamic identification of the structure.

Fig. 28 shows the general block diagram of the proposed dynamic analysis procedure, which could be considered a proper way to evaluate the influence of a viscous damper on the structure, as well as could help to design it. The first stage of the analysis should be the development of a complex FEM model that would describe the design structure as accurately as possible to determine the basic dynamic parameters such as eigenfrequencies and eigenvectors. If the frequencies are not in the critical range, it can be assumed that the bridge will fulfill all service requirements. When the frequency is in the range up to 5 Hz, the complex dynamic analysis should be performed [82]. Due to the time-consuming computations, it is recommended to create a simplified model. This model should be subjected to an iterative validation process. As result, the dynamic parameters such as eigenfrequencies and eigenvectors should be close to those reached in the complex model. After compliance with the interesting parameters, the simplified model should be subjected to various human-induced loadings. Based on the obtained acceleration results, the comfort criteria can be examined; if

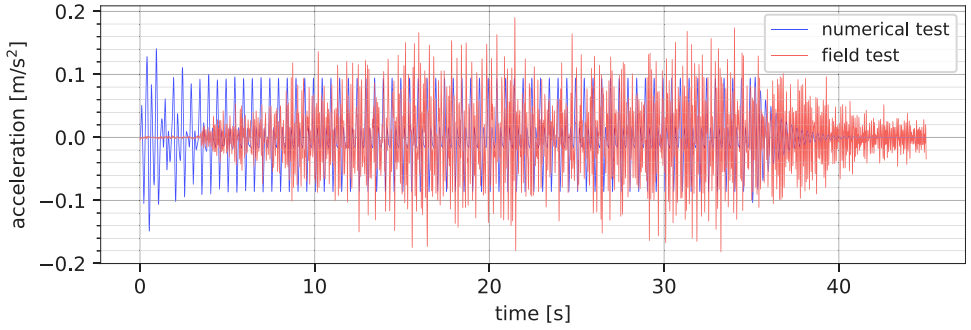

(a)

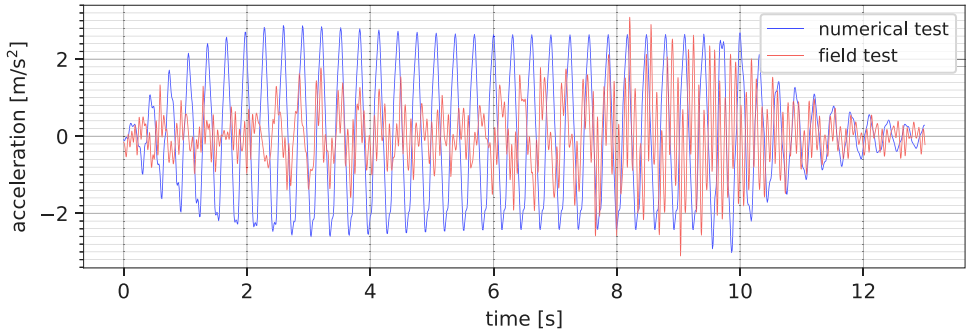

(b)

Fig. 27. Comparison of the time history accelerations obtained by the numerical model M-02D and the field test: (a) Response under free march; (b) response under the squatting.

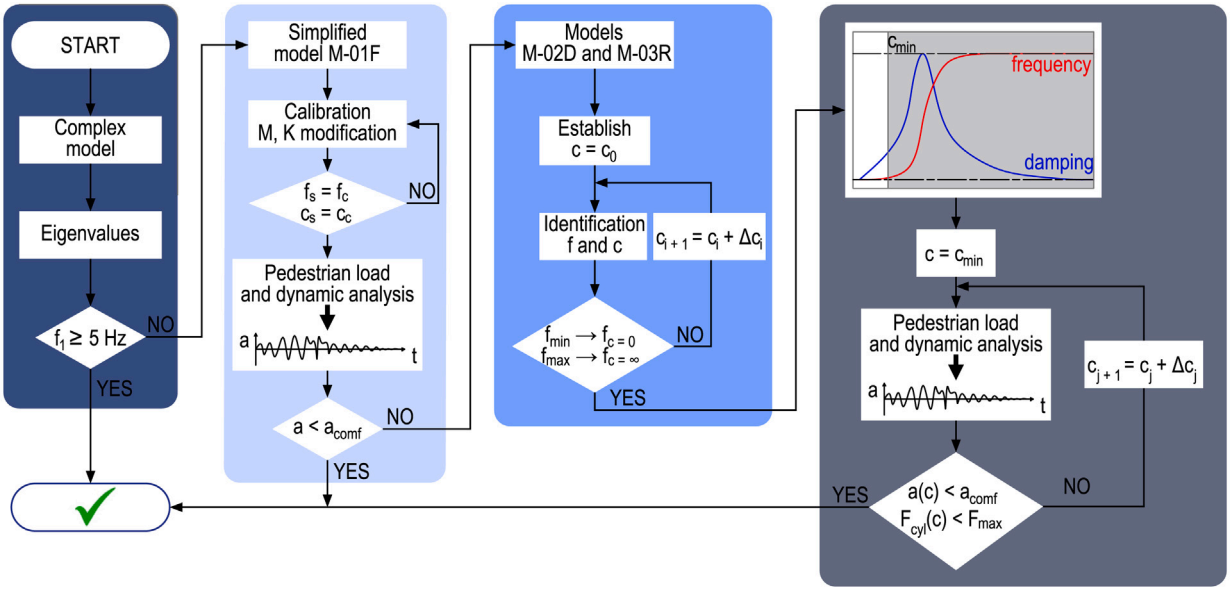

Fig. 28. Flowchart of the developed procedure allowing to estimate the damper constant required to reduce excessive vibrations and to shift the natural frequency.

the acceleration and frequency values provide comfort conditions, this completes the analysis. The comfort criteria are often not fulfilled at this stage of the calculation, which therefore requires modifications to reduce the acceleration level. One of the solutions is introducing an additional viscous damper to the structure. In the case of a drawbridge, it can be an economical way to modify its dynamic characteristics. This should allow the frequency of the natural vibrations to be shifted from the range associated with human-induced vibration and to reduce the acceleration of the structure. In the first stage, it is recommended to make simplified numerical models with different boundary conditions. One of the numerical models (M-02D) should have an additional damping element, and the other model (M-03R) in place of a viscous damper should have rigid support. The next step is to perform the iterative calculation procedure. Calculations with increasing the damper

constant at each step should be performed with the M-02D numerical model. The initial value should not induce any significant change of the natural frequencies, as in M-01F. In each step, for model M-02D, the analysis of the free response of the structure should be performed. Then, the modal analysis technique should be utilized to determine the natural frequencies, damping, and modal shapes. After conducting a full iterative analysis, a graph of the structure's natural frequency and modal damping depending on the additional damper constant can be obtained, as shown in Fig. 15. The next step is to select the minimum damper coefficient that causes a frequency change. Then, the model with the adopted minimum additional damping should be subjected to the iterative procedure, which includes the determination of the maximal accelerations under human-induced loading. The damper constant should be increased, starting from the adopted minimum value. The range of the damper constant, where the maximal accelerations and force in a cylinder are acceptable, should be defined; this range may be adopted as a guideline for the damping device's manufacturer. The dynamic load on the cylinder comes only from the dynamic component of the footbridge load and can be estimated at 5% of the value of the code load.

The proposed procedure applies only to the selected types of structures. If despite the applied damping and the execution of the proposed procedure, the footbridge still does not fulfill the comfort criteria, a change of the geometry or the location of the damping devices should be performed.

6. Conclusions

Dampers are usually used to increase the damping of a structure. This paper presents a conducted comprehensive research in order to implement the idea of the use of a viscous damper which modifies the boundary conditions of static schema and in consequence the natural frequency of a pedestrian drawbridge. It allowed eliminating the problem of pedestrian discomfort caused by excessive vibration. The idea was studied using a simple mechanical model. The parametric solution of the equation of motion confirmed the usefulness of the method. It was demonstrated using the FEM model that, in a particular case, the range of natural frequencies of the span can be changed by using an additional viscous damper with a high damper coefficient. It should be emphasized that in such a case where nonproportional damping occurs, the modal parameters cannot be determined with the generalized or standard eigenvalue problem commonly implemented in commercial programs. The appropriate value of the damper constant was determined based on parametric dynamic analysis using direct integration of the equation of motion. Finally, the first natural frequency was shifted from 1.64 to 3.13 Hz. Based on the presented research, changes were made to the bridge's driving system under construction. To the best of the authors' knowledge, this is the first implementation of this idea in a bridge structure. The developed procedure allowed to estimate the damper coefficient required to reduce excessive vibrations and to shift the natural frequency. The correctness of the assumptions was finally confirmed by a field test. The level of pedestrian comfort was evaluated as the first class based on the acceleration results obtained from the numerical analysis and the field test. Nevertheless, the following activities could improve the consistency of the theoretical and field results. First, the structural damping of the bridge could be confirmed under construction when the span is not connected to the driving cylinders. Second, the possibility of delivering the driving hydraulic cylinders with a precise damper coefficient could be beneficial, because it would allow introducing optimization in the damper coefficient's selection process.

The most important element of the presented solution is the fact that the static system modified by the damper works only under the dynamic component of the load. Thanks to this, the forces acting on the damper components are small. Adaptation of the driving cylinder to the role of the viscous damper, which acts in service, proved to be favorable. It should be emphasized that a passive hydraulic cylinder would also introduce damping into the system. However, the procedure presented in this paper provides predictable results. This method is not universal but can be an inspiration during designing new constructions. It also allows to design economically and aesthetically, heretofore designers have often increased cross-sections to improve the dynamic behavior of the structure.

CRediT authorship contribution statement

Krzysztof Zoltowski: Methodology, Investigation, Writing – review & editing, Supervision. **Anna Banas:** Measurements, Data processing, Writing – original draft. **Mikolaj Binczyk:** Dynamic analysis, Writing – original draft. **Przemyslaw Kalitowski:** Modal analysis, Software, Writing – original draft, Visualization.

Declaration of competing interest

The authors declare that they have no known competing financial interests or personal relationships that could have appeared to influence the work reported in this paper.

References

[1] Zoltowski K, Binczyk M, Kalitowski P. Footbridges. In: Dynamic design–selected problems. Footbridge 2017 berlin, Chair of Conceptual and Structural Design, Fachgebiet Entwerfen und Konstruieren – Massivbau, Technische Universität Berlin; 2017, p. 7–9. http://dx.doi.org/10.24904/footbridge2017.09357, (September 2017).

[2] Binczyk M, Żółtowski K. Launching of steel bridge girder. Application of nonlinear shell models, CRC Press Taylor & Francis/Balkema; 2019.

[3] Živanović S, Pavic A, Reynolds P. Finite element modelling and updating of a lively footbridge: The complete process. J Sound Vib 2007;301(1–2):126–45. http://dx.doi.org/10.1016/j.jsv.2006.09.024.

[4] Żółtowski K, Binczyk M. Arch Footbridge over Warta River in Wronki - Design and Construction. Dolnośląskie Wydawnictwo Edukacyjne; 2016, p. 380–3.

[5] Malinowski M, Banaś A, Jeszka M, Sitarski A. Original footbridge in mikolajki, Poland. STAHLBAU 2018;87:248–55. http://dx.doi.org/10.1002/stab.201810582.

[6] Banas A, Jankowski R. Experimental and numerical study on dynamics of two footbridges with different shapes of girders. Appl Sci 2020;10(13):4505.

[7] Dallard P, Fitzpatrick T, Flint A, Low A, Smith RR, Willford M, Roche M, Ridsdill Smith R, Willford M, Roche M. London Millennium bridge: Pedestrian-induced lateral vibration. J Bridge Eng 2001;6(6):412–7. http://dx.doi.org/10.1061/(ASCE)1084-0702(2001)6:6(412).

[8] Dallard P, Fitzpatrick T, Flint A, Bourva S, Low A, Ridsdill R, Willford M, Fitzpatrick AJ, Flint A, Le Bourva S, Low A, Ridsdill Smith RM, Willford M. The London millennium footbridge. Struct Eng 2001;79(22):17–33.

[9] Blekherman AN. Autoparametric resonance in a pedestrian steel arch bridge: Solferino bridge, Paris. J Bridge Eng 2007;12(6):669.

[10] Dziuba P, Grillaud G, Flamand O, Sanquier S, Tétard Y. La passerelle solférino comportement dynamique (dynamic behaviour of the solférino bridge). Bull Ouvrages Métall 2001;1:34–57.

[11] Živanović S, Pavic A, Reynolds P. Vibration serviceability of footbridges under human-induced excitation: a literature review. J Sound Vib 2005;279(1–2):1–74. http://dx.doi.org/10.1016/j.jsv.2004.01.019.

[12] Zoltowski K. Footbridges, numerical approach. In: Caetano E, Cunha A, Hoorpah W, Raoul J, editors. Footbridge vibration design. Leiden, Netherlands: CRC Press/Balkema; 2009, p. 54–70.

[13] Bachmann H. Case studies of structures with man-induced vibrations. J Struct Eng 1992;118(3):631.

[14] Zoltowski K. Dynamic properties of lively footbridge. Tuning the structure. In *Footbridge 2014: Past, present and future. [5th international conference]*, London, 2014.

[15] Feldmann M, Heinemeyer C, Lukic M, Caetano E, Cunha A, Goldack A, Keil A, Schlaich M, Hicks S, Smith A, Hechler O, Obiala R, Galanti F, Waarts P. Human-induced vibration of steel structures (hivoss). EUR research fund for coal and steel. Luxembourg: Off. for Official Publ. of the European Communities; 2010, p. 20. http://dx.doi.org/10.2777/79056.

[16] Van Nimmen K, Lombaert G, De Roeck G, Van den Broeck P. Vibration serviceability of footbridges: Evaluation of the current codes of practice. Eng Struct 2014;59:448–61. http://dx.doi.org/10.1016/j.engstruct.2013.11.006.

[17] Bachmann H, Weber B. Tuned vibration absorbers for "lively" structures. Struct Eng Int 1995;5(1):31–6. http://dx.doi.org/10.2749/101686695780601457.

[18] Reiterer M, Ziegler F. Control of pedestrian-induced vibrations of footbridges using tuned liquid column dampers. 2004.

[19] Kandemir EC, Mazda T, Nurui H, Miyamoto H. Seismic retrofit of an existing steel arch bridge using viscous damper. Procedia Eng 2011;14:2301–6. http://dx.doi.org/10.1016/j.proeng.2011.07.290.

[20] Xu X, Li Z, Liu W, Feng D, Li X. Investigation of the wind-resistant performance of seismic viscous dampers on a cable-stayed bridge. Eng Struct 2017;145:283–92. http://dx.doi.org/10.1016/j.engstruct.2017.05.008.

[21] Kye S, Jung H-JJH-YY, Jung H-JJH-YY. Experimental investigation on a cable structure equipped with an electrodynamic damper and its monitoring strategy through energy harvesting. Sensors 2019;19(11):2631. http://dx.doi.org/10.3390/s19112631.

[22] Preumont AA, Voltan M, Sangiovanni A, Mokrani B, Alaluf D. Active tendon control of suspension bridges. Smart Struct Syst 2016;18(1):31–52. http://dx.doi.org/10.12989/sss.2016.18.1.031.

[23] Wang D, Wu C, Zhang Y, Li S. Study on vertical vibration control of long-span steel footbridge with tuned mass dampers under pedestrian excitation. J Construct Steel Res 2019;154:84–98. http://dx.doi.org/10.1016/j.jcsr.2018.11.021.

[24] Qin S, Zhou Y-LL, Kang J. Footbridge serviceability analysis: From system identification to tuned mass damper implementation. KSCE J Civ Eng 2019;23(2):754–62. http://dx.doi.org/10.1007/s12205-018-0985-7.

[25] Tubino F, Piccardo G. Tuned mass damper optimization for the mitigation of human-induced vibrations of pedestrian bridges. Meccanica 2015;50(3):809–24. http://dx.doi.org/10.1007/s11012-014-0021-z.

[26] Caetano E, Cunha A, Moutinho C, Magalhães F. Studies for controlling human-induced vibration of the pedro e inês footbridge, Portugal. Part 2: Implementation of tuned mass dampers. Eng Struct 2010;32(4):1082–91. http://dx.doi.org/10.1016/j.engstruct.2009.12.033.

[27] Di Matteo A, Masnata C, Pirrotta A. Simplified analytical solution for the optimal design of tuned mass damper inerter for base isolated structures. Mech Syst Signal Process 2019;134:106337. http://dx.doi.org/10.1016/j.ymssp.2019.106337.

[28] Weber F. Semi-active vibration absorber based on real-time controlled mr damper. Mech Syst Signal Process 2014;46(2):272–88. http://dx.doi.org/10.1016/j.ymssp.2014.01.017.

[29] Maślanka M. Optimised semi-active tuned mass damper with acceleration and relative motion feedbacks. Mech Syst Signal Process 2019;130:707–31. http://dx.doi.org/10.1016/j.ymssp.2019.05.025.

[30] Ferreira F, Moutinho C, Cunha A, Caetano E. Use of semi-active tuned mass dampers to control footbridges subjected to synchronous lateral excitation. J Sound Vib 2019;446:176–94.

[31] Lin CC, Wang JF, Chen BL. Train-induced vibration control of high-speed railway bridges equipped with multiple tuned mass dampers. J Bridge Eng 2005;10(4):398–414. http://dx.doi.org/10.1061/(ASCE)1084-0702(2005)10:4(398).

[32] Li H-NN, Ni X-LL. Optimization of non-uniformly distributed multiple tuned mass damper. J Sound Vib 2007;308(1–2):80–97. http://dx.doi.org/10.1016/j.jsv.2007.07.014.

[33] Vellar LS, Ontiveros-Pérez SP, Miguel LFF, Fadel Miguel LF. Robust optimum design of multiple tuned mass dampers for vibration control in buildings subjected to seismic excitation. Shock Vib 2019;2019:1–9. http://dx.doi.org/10.1155/2019/9273714.

[34] Li Q, Fan J, Nie J, Li Q, Chen Y. Crowd-induced random vibration of footbridge and vibration control using multiple tuned mass dampers. J Sound Vib 2010;329(19):4068–92. http://dx.doi.org/10.1016/j.jsv.2010.04.013.

[35] Moutinho C, Cunha, Caetano E, de Carvalho JM, Cunha A, Caetano E, de Carvalho JM. Vibration control of a slender footbridge using passive and semiactive tuned mass dampers. Struct Control Health Monit 2018;25(9):e2208. http://dx.doi.org/10.1002/stc.2208.

[36] Zhang L, Huang JY. Dynamic interaction analysis of the high-speed maglev vehicle/guideway system based on a field measurement and model updating method. Eng Struct 2019;180(December 2017):1–17. http://dx.doi.org/10.1016/j.engstruct.2018.11.031.

[37] Pradelok S, Jasiński M, Kocański T, Poprawa G. Numerical determination of dynamic response of the structure on the example of arch bridge. Procedia Eng 2016;161:1084–9. http://dx.doi.org/10.1016/j.proeng.2016.08.852.

[38] Caetano E, Cunha A, Magalhães F, Moutinho C. Studies for controlling human-induced vibration of the pedro e inês footbridge, Portugal. Part 1: Assessment of dynamic behaviour. Eng Struct 2010;32(4):1069–81. http://dx.doi.org/10.1016/j.engstruct.2009.12.034.

[39] Drygala IJ, Dulinska JM. Full-scale experimental and numerical investigations on the modal parameters of a single-span steel-frame footbridge. Symmetry 2019;11(3):404. http://dx.doi.org/10.3390/sym11030404.

[40] Magalhães F, Cunha A, Caetano E, Brincker R. Damping estimation using free decays and ambient vibration tests. Mech Syst Signal Process 2010;24(5):1274–90. http://dx.doi.org/10.1016/j.ymssp.2009.02.011.

[41] Pavic A, Armitage T, Reynolds P, Wright J. Methodology for modal testing of the millennium bridge, London. Proc Inst Civ Eng - Struct Build 2002;152(2):111–21. http://dx.doi.org/10.1680/stbu.2002.152.2.111.

[42] Chróścielewski J, Miśkiewicz M, Pyrzowski Ł, Rucka M, Sobczyk B, Wilde K. Modal properties identification of a novel sandwich footbridge – comparison of measured dynamic response and FEA. Composites B 2018;151(May):245–55. http://dx.doi.org/10.1016/j.compositesb.2018.06.016.

[43] Gręboswki K, Rucka M, Wilde K. Non-destructive testing of a sport tribune under synchronized crowd-induced excitation using vibration analysis. Materials 2019;12(13):2148. http://dx.doi.org/10.3390/ma12132148.

[44] Maia NMM, Silva JMM. Modal analysis identification techniques. Phil Trans R Soc A 2001;359(1778):29–40.

[45] Bagheri A, Ozbulut OE, Harris DK. Structural system identification based on variational mode decomposition. J Sound Vib 2018;417:182–97.

[46] Brownjohn J, Au S-KK, Li B, Bassitt J. Optimised ambient vibration testing of long span bridges. Procedia Eng 2017;199:38–47. http://dx.doi.org/10.1016/j.proeng.2017.09.147.

[47] Brincker R, Ventura CE. Introduction to operational modal analysis. Chichester, West Sussex: Wiley; 2015, p. 1–360. http://dx.doi.org/10.1002/9781118535141.

[48] Rainieri C, Fabbrocino G. Operational modal analysis of civil engineering structures: an introduction and guide for applications. Italy, Europe: Springer-Verlag; 2014.

[49] Brownjohn JMW, Magalhaes F, Caetano E, Cunha A. Ambient vibration re-testing and operational modal analysis of the humber bridge. Eng Struct 2010;32(8):2003–18. http://dx.doi.org/10.1016/j.engstruct.2010.02.034.

[50] Magalhães F, Cunha A, Caetano E. Vibration based structural health monitoring of an arch bridge: From automated OMA to damage detection. Mech Syst Signal Process 2012;28:212–28. http://dx.doi.org/10.1016/j.ymssp.2011.06.011.

[51] Adhikari S. Optimal complex modes and an index of damping non-proportionality. Mech Syst Signal Process 2004;18(1):1–27. http://dx.doi.org/10.1016/S0888-3270(03)00048-7.

[52] Prandina M, Mottershead JE, Bonisoli E. An assessment of damping identification methods. J Sound Vib 2009;323(3–5):662–76. http://dx.doi.org/10.1016/j.jsv.2009.01.022.

[53] Inman DJ, Lallement G. A Tutorial on complex eigenvalues. In *Proceedings of spie - the international society for optical engineering, no. January 1995*, 1995, p. 7.

[54] Charney FA, McNamara RJ. Comparison of methods for computing equivalent viscous damping ratios of structures with added viscous damping. J Struct Eng 2008;134(1):32–44. http://dx.doi.org/10.1061/(ASCE)0733-9445(2008)134:1(32).

[55] Lázaro M, Pérez-Aparicio JL, Epstein M. A viscous approach based on oscillatory eigensolutions for viscoelastically damped vibrating systems. Mech Syst Signal Process 2013;40(2):767–82. http://dx.doi.org/10.1016/j.ymssp.2013.06.005.

[56] Suarez LE, Gaviria CA. Dynamic properties of a building with viscous dampers in non-proportional arrangement. Struct Eng Mech 2015;55(6):1241–60. http://dx.doi.org/10.12989/sem.2015.55.6.1241.

[57] Lee D, Taylor DP. Viscous damper development and future trends. Struct Des Tall Build 2001;10(5):311–20. http://dx.doi.org/10.1002/tal.188.

[58] Losanno D, Londono JM, Zinno S, Serino G. Effective damping and frequencies of viscous damper braced structures considering the supports flexibility. Comput Struct 2018;207:121–31. http://dx.doi.org/10.1016/j.compstruc.2017.07.022.

[59] Losanno D, Spizzuoco M, Serino G. Design and retrofit of multistory frames with elastic-deformable viscous damping braces. J. Earthq Eng 2019;23(9):1441–64. http://dx.doi.org/10.1080/13632469.2017.1387193.

[60] Whittle JK, Williams MS, Karavasilis TL, Blakeborough A. A comparison of viscous damper placement methods for improving seismic building design. J. Earthq Eng 2012;16(4):540–60. http://dx.doi.org/10.1080/13632469.2011.653864.

[61] de Lima AMG, Rade DA, Lépore Neto FP. An efficient modeling methodology of structural systems containing viscoelastic dampers based on frequency response function substructuring. Mech Syst Signal Process 2009;23(4):1272–81. http://dx.doi.org/10.1016/j.ymssp.2008.09.005.

[62] Lewandowski R, Bartkowiak A, Maciejewski H. Dynamic analysis of frames with viscoelastic dampers: a comparison of damper models. Struct Eng Mech 2012;41(1):113–37. http://dx.doi.org/10.12989/sem.2012.41.1.113.

[63] Carrie TG. Guy cable design and damping for vertical axis wind turbines. NASA. Lewis Research Center Wind Turbine Dyn.; 1981, p. 255–64.

[64] Caracoglia L, Jones NP. Damping of taut-cable systems: Two dampers on a single stay. J Eng Mech 2007;133(10):1050–60. http://dx.doi.org/10.1061/(ASCE)0733-9399(2007)133:10(1050).

[65] Cu VH, Han B, Pham DH, Yan WT. Free vibration and damping of a taut cable with an attached viscous mass damper. KSCE J Civ Eng 2018;22(5):1792–802. http://dx.doi.org/10.1007/s12205-017-1167-8.

[66] Hairer E, Wanner G. Solving ordinary differential equations ii. stiff and differential-algebraic problems. Berlin, Switzerland, Europe: Springer; 1996.

[67] Newmark NM. A method of computation for structural dynamics. J Eng Mech Div 1959;85(3):67–94.

[68] Chopra AK. Dynamics of structures: theory and applications to earthquake engineering. fourth ed.. Upper Saddle River, N.J: Prentice Hall; 2012, p. 944.

[69] SOFiSTiK. ASE general static analysis of finite element structures. ASE manual, version 2018-8 software version SOFiSTiK 2018, 2018.

[70] Zoltowski K. Pedestrian bridge. Load and response. In *Proceedings of the second international conference footbridges 2005*, 2005, p. 247–8.

[71] Matsumoto Y, Shiojiri H, Nishioka T, Shiojiri H, Matsuzaki K. Dynamic design of footbridges. IABSE Proc 1978;2(17):1–15. http://dx.doi.org/10.5169/SEALS-33221.
[72] Alvin KF, Robertson AN, Reich GW, Park KC. Structural system identification: from reality to models. Comput Struct 2003;81(12):1149–76. http://dx.doi.org/10.1016/S0045-7949(03)00034-8.
[73] Ewins DJ. Modal testing: theory, practice and application. Baldock: RESEARCH STUDIES PRESS LTD.; 2000.
[74] Pappa RS, Juang JN. An eigensystem realization algorithm (ERA) for modal parameter identification and model reduction. In: JPL proc. of the workshop on identification and control of flexible space struct., Vol. 3. 1985.
[75] Juang J-NJN, Suzuki H, Juang J-NJN. An eigensystem realization algorithm in frequency domain for modal parameter identification. Astrodyn Conf 1986;1986(2). http://dx.doi.org/10.2514/6.1986-2048.
[76] Li P, Hu SLJ, Li HJ. Noise issues of modal identification using eigensystem realization algorithm. Procedia Eng 2011;14:1681–9. http://dx.doi.org/10.1016/j.proeng.2011.07.211.
[77] Schutter B, De Schutter B. Minimal state-space realization in linear system theory: an overview. J Comput Appl Math 2000;121(1–2):331–54. http://dx.doi.org/10.1016/S0377-0427(00)00341-1.
[78] Caicedo JM. Practical guidelines for the natural excitation technique (next) and the eigensystem realization algorithm (ERA) for modal identification using ambient vibration. Exp Tech 2011;35(4):52–8. http://dx.doi.org/10.1111/j.1747-1567.2010.00643.x.
[79] Allemang RJ. The modal assurance criterion—Twenty years of use and abuse.. Sound Vib 2003;37(8):14–23.
[80] Pappa RS, Elliott KB, Schenk A. A consistent-mode indicator for the eigensystem realization algorithm. Hampton, Va., Springfield, Va.: National Aeronautics and Space Administration, Langley Research Center ; For sale by the National Technical Information Service, 1992; 1992.
[81] Sétra. Footbridges - assessment of vibrational behaviour of footbridges under pedestrian loading. 2006, p. 127, (october).
[82] PKN. EN 1990:2002 eurocode - basis of structural design. European committee for standarization; 2002.